



Cite this: *Org. Biomol. Chem.*, 2018, **16**, 3824

## Time-lapse monitoring of TLR2 ligand internalization with newly developed fluorescent probes†

Yohei Arai,<sup>a</sup> Kouhei Yokoyama,<sup>b</sup> Yuki Kawahara,<sup>b</sup> Qi Feng,<sup>b</sup> Ippei Ohta,<sup>a</sup> Atsushi Shimoyama,<sup>b</sup> Shinsuke Inuki,<sup>‡a</sup> Koichi Fukase,<sup>b</sup> Kazuya Kabayama<sup>\*,b</sup> and Yukari Fujimoto<sup>\*,a</sup>

As a mammalian toll-like receptor family member protein, TLR2 recognizes lipoproteins from bacteria and modulates the immune response by inducing the expression of various cytokines. We have developed fluorescence-labeled TLR2 ligands with either hydrophilic or hydrophobic fluorescence groups. The labeled ligands maintained the inflammatory IL-6 induction activity and enabled us to observe the internalization and colocalization of the TLR2 ligands using live-cell imaging. The time-lapse monitoring in the live-cell imaging of the fluorescence-labeled TLR2 ligand showed that TLR2/CD14 expression in the host cells enhanced the internalization of TLR2 ligand molecules.

Received 30th December 2017,  
Accepted 2nd May 2018

DOI: 10.1039/c7ob03205f

rsc.li/obc

### Introduction

Bacterial membrane lipoproteins are recognized by an innate immune receptor, toll-like receptor 2 (TLR2), a type I transmembrane glycoprotein. TLR2 recognizes the ligands along with TLR1 or TLR6, forming homo- or heterodimers that modulate the immune system.<sup>1,2</sup> In some cases, distinct lipoproteins/lipopeptides are recognized by TLR2 in a TLR1- and TLR6-independent manner.<sup>3</sup> Activation of TLR2 results in induction of various inflammatory cytokines, including interleukin-6 (IL-6), IL-8 and tumor necrosis factor alpha (TNF- $\alpha$ ). The immunomodulatory activity *via* cytokine induction leads to establishment of adaptive immunity. Hence, TLR2 ligands are important candidates for immune adjuvants in vaccine development,<sup>4,5</sup> including in cancer immunotherapy.<sup>6–9</sup>

One of the representative TLR2 ligands is bacterial lipoprotein/lipopeptide, which typically has a diacylglycerol moiety linked to the thiol group of cysteine at the N-terminus of the protein, occasionally along with an additional acyl group at the N-terminus of the cysteine (*i.e.* triacyl lipoproteins). The lipoproteins in most Gram-negative bacteria are triacylated,<sup>10</sup>

whereas in some Gram-positive bacteria and mycoplasma, the lipoproteins are diacylated.<sup>11–13</sup> The triacyl lipoproteins are recognized by TLR1/2 heterodimers, whereas diacyl lipoproteins are generally recognized by TLR2/6 heterodimers. After the finding of lipoproteins/peptides as TLR2 ligands in mycoplasma<sup>14</sup> and Gram-negative bacteria,<sup>15–17</sup> lipoproteins from *Staphylococcus aureus* were also found as TLR2 ligands in Gram-positive bacteria,<sup>11,12,18</sup> and various types of bacterial lipoprotein structures including lyso-type diacylated structures from Gram-positive bacteria were also reported.<sup>13</sup>

In the investigation of the detailed cellular functions of the TLR2 ligand in host cells, cellular imaging studies using labeled ligands, especially fluorescence-labeled molecules, have played important roles.

As for the investigation on the intracellular localization of the receptor TLR2, several groups reported the internalization.<sup>19–25</sup> Vasselon *et al.*, for example, used a fluorescence-labeled triacylated lipopeptide ligand to show colocalization with TLR2 using confocal microscopy.<sup>19</sup> Some reports suggested that TLR2 signaling occurs in lipid rafts<sup>22,23</sup> or at plasma membranes.<sup>24</sup> Several reports also showed that the internalization of TLR2 plays a fundamental role in the immune responses along with CD14.<sup>25–30</sup> On the other hand, the imaging of the fluorescence-labeled TLR2 ligand was also used to detect pancreatic cancer<sup>31</sup> as TLR2 is highly expressed in 70% of pancreatic tumors.<sup>31</sup>

As aforementioned, the cellular imaging studies of TLR2 have been performed and have contributed to the understanding of TLR2 functions, but the analyses were mostly conducted under static conditions. In order to observe cellular

<sup>a</sup>Faculty of Science and Technology, Keio University, Hiyoshi 3-14-1, Yokohama, Kanagawa 223-8522, Japan. E-mail: fujimotoy@chem.keio.ac.jp

<sup>b</sup>Graduate School of Science, Osaka University, Machikaneyama 1-1, Toyonaka, Osaka 560-0043, Japan. E-mail: kaba@chem.sci.osaka-u.ac.jp

†Electronic supplementary information (ESI) available. See DOI: 10.1039/c7ob03205f

‡Present address: Graduate School of Pharmaceutical Sciences, Kyoto University, Sakyo-ku, Kyoto 606-8501, Japan.

phenomena and the dynamics of living cells, especially ligand internalization by cells either expressing TLR2/CD14 or not, live-cell imaging techniques using time-lapse microscopy would provide substantially more visual information as one of the visualization technologies. In live-cell imaging analysis, there is significant value in the continuous observation while focusing on several certain cells for a long time. However, a relatively high concentration of fluorescence-labeled lipopeptides has been required for live cell imaging so far. Under these conditions, nonspecific uptake may also be observed owing to the lipophilic character of lipopeptides.

In this research, we planned to visualize the dynamics of the labeled-ligand in host cells with or without TLR2/CD14 expression, under physiologically relevant conditions at the lower concentration, to prevent the nonspecific uptake (Fig. 1). We thus first planned to develop fluorescence-labeled lipopeptides as TLR2 ligands that retain their biological activities and can be used for the live-cell imaging. For developing the fluorescence-labeled TLR2 ligands, we introduced hydrophilic (Alexa Fluor® 594 and TAMRA) and hydrophobic groups (stilbene-type and tolan-type). We also introduced a stilbene-type fluorophore into the N-terminal of the lipopeptide instead of a fatty acid of Pam<sub>2</sub>CSK<sub>4</sub>. Using the newly developed fluorescence-labeled TLR2 ligands, we proceeded to visualize the dynamics of the labeled-ligand in host cells with or without the receptor protein expression at the lower concentration. These analyses were planned by using the confocal microscope system equipped with a highly sensitive GaAsP detector.

## Results and discussion

### Synthesis of fluorescence-labeled TLR2 ligands

We first synthesized bacterial lipopeptide fluorescent probes as TLR2 ligands, which have a Pam<sub>2</sub>CSK<sub>4</sub> backbone equipped with or without a linker (linker: Cys–Lys) to introduce a fluorescent group (Scheme 1). Four fluorescent groups with different types of structures, including Alexa Fluor® 594, TAMRA, a stilbene derivative, and a tolan derivative, were used as either hydrophilic or hydrophobic groups to compare the immunostimulatory activities of the resulting fluorescent

ligands. In order to synthesize the peptide part of the labeled ligands, Rink Amide (RAM) resin was used as the solid support for solid-phase peptide synthesis.

Before introducing the peptide moiety of the Pam<sub>2</sub>CSK<sub>4</sub>, the linker was introduced to the resin; for the preparation of the linker, *N*-α-(9-fluorenylmethoxycarbonyl)-*N*-ε-[1-(4,4-dimethyl-2,6-dioxocyclohexylidene)ethyl]-*L*-lysine (Fmoc-*L*-Lys(Dde)OH) was first introduced into the RAM resin using *N,N'*-diisopropylcarbodiimide (DIC) and 1-hydroxybenzotriazole (HOBT) in THF, and then the cysteine residue (Boc-*L*-Cys(Trt)-OH) was subsequently joined to Lys to generate the linker moiety supported on the resin. After removal of the Dde group of Lys with hydrazine hydrate in *N,N*-dimethylformamide (DMF), the linker supported with the RAM resin was obtained. The peptide part of the TLR2 ligand, Ser-(Lys)<sub>4</sub>, was then introduced by stepwise elongation using Fmoc solid-phase peptide synthesis. Next, the Fmoc-Pam<sub>2</sub>Cys-OH was reacted under the same amide formation conditions, DIC and HOBT in DMF. During cleavage of the lipopeptide from the solid support, the trityl group on the cysteine was also removed to give lipopeptide. The thiol group of the key intermediate 3 (Pam<sub>2</sub>CSK<sub>4</sub>-linker-NH<sub>2</sub>) was reacted with fluorescent groups with maleimide linkers to give the fluorescence-labeled compounds 1a–1d. The compounds were purified using reverse-phase HPLC analysis as described in the ESI.†

We also synthesized the fluorescence labeled (stilbene-type) compound at the N-terminus of Pam<sub>2</sub>CSK<sub>4</sub>, shown as 1e. The detailed synthetic pathway is described in the ESI.†

**Inflammatory cytokine induction by synthesized fluorescence-labeled ligands.** To evaluate the immunostimulatory activities of the fluorescence-labeled compounds that we synthesized, 1a–1e, we analyzed an inflammatory cytokine. Hence, IL-6 induction depending on the synthesized compounds was determined in human and murine macrophage cell lines (Fig. 2).<sup>32</sup> Namely, the phorbol 12-myristate 13-acetate (PMA)-differentiated THP-1 human monocytic cells and mouse macrophage RAW 264.7 cells were used for the analysis (Fig. 2). By measuring IL-6 induction in THP-1 cells (Fig. 2A), we determined that all five labeled compounds 1a–1e showed satisfactory activities as fluorescent probes, although they were relatively less active than unlabeled Pam<sub>2</sub>CSK<sub>4</sub>. In mouse macrophage RAW 264.7 cells (Fig. 2B), the trend of the observed activities was similar to the results we obtained with THP-1. Compounds 1a–1e maintained their IL-6 induction activities in both human (PMA-differentiated THP-1) and mouse (RAW 264.7) cells, and some compounds, especially 1a in murine macrophage RAW 264.7 cells, showed relatively higher activity than the unmodified Pam<sub>2</sub>CSK<sub>4</sub>, while the fluorescence labeling of other compounds caused a slight reduction in measured activity. Among the synthesized compounds, Alexa Fluor® 594-labeled lipopeptide 1a showed the highest immunostimulation, and it is noteworthy that the ligands containing lipophilic rod-shaped fluorescent groups, 1c, 1d and 1e, also maintained their activities. We therefore utilized 1a and 1e as the fluorescent probes for the live-cell imaging analysis.

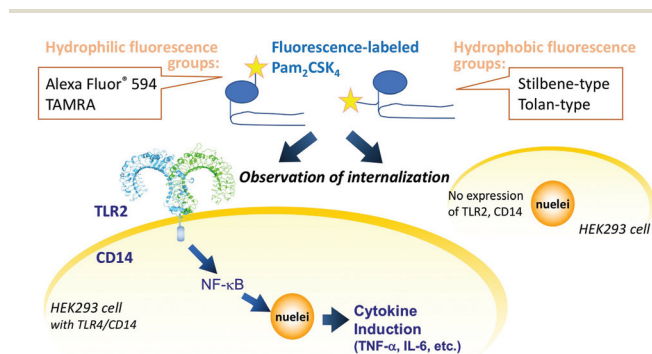
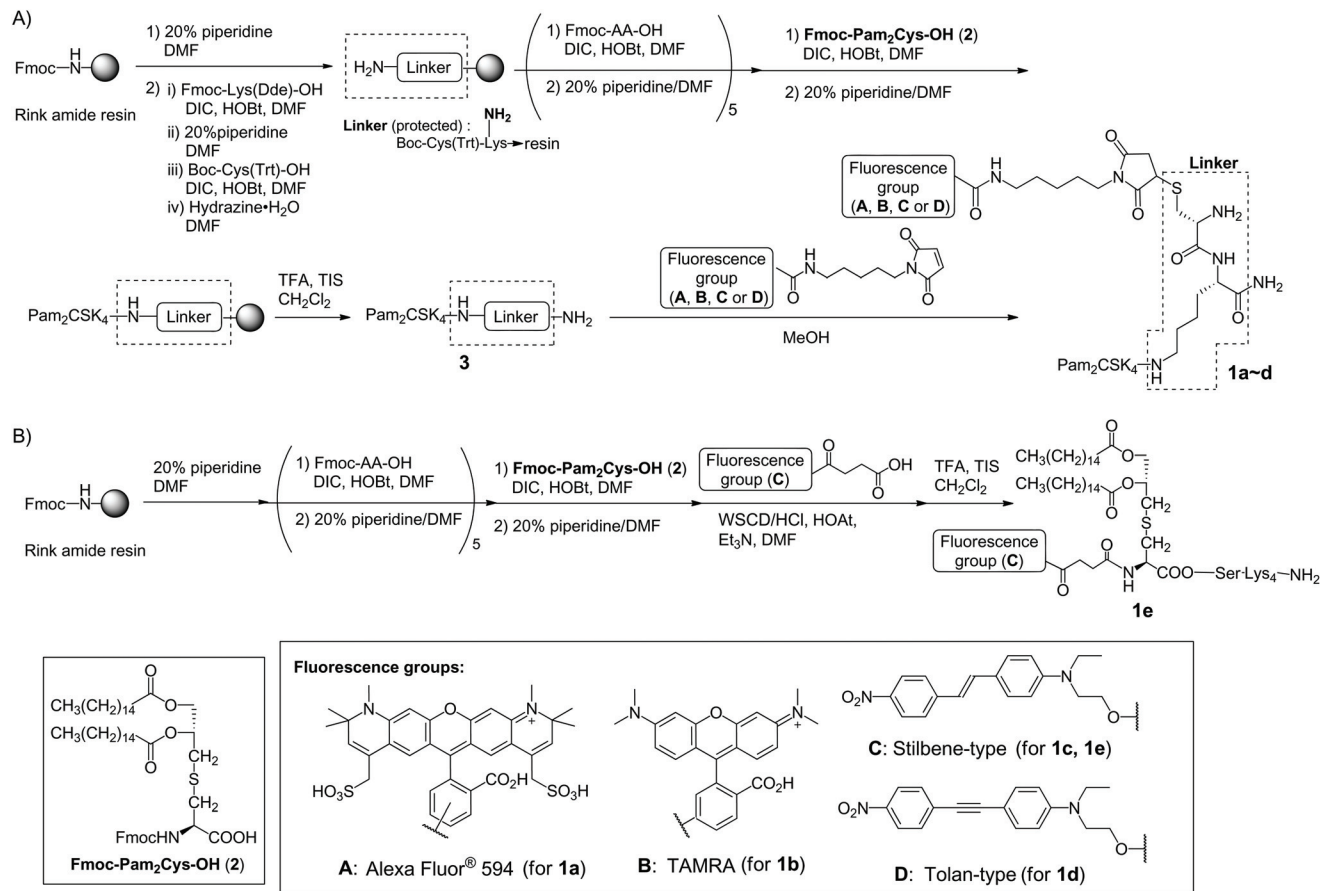
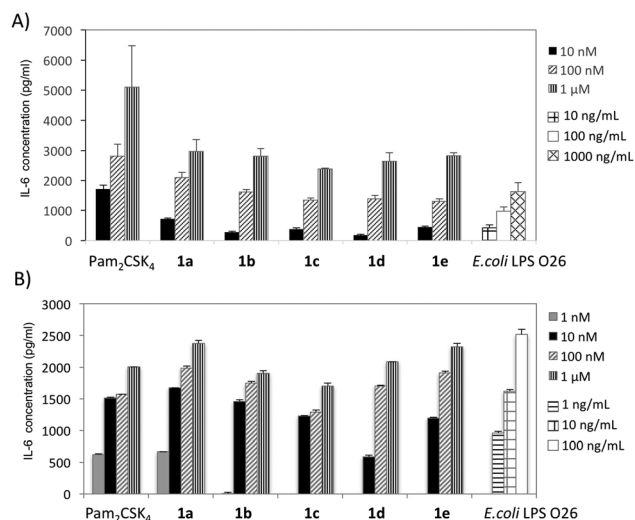


Fig. 1 Fluorescence-labeled TLR2 ligands (Pam<sub>2</sub>CSK<sub>4</sub>) for the time-lapse monitoring of TLR2 ligand internalization.



**Scheme 1** Synthesis of fluorescence-labeled TLR2 ligands **1a–1e**.



**Fig. 2** Proinflammatory cytokine inductions by synthesized compounds **1a–1e**. (A) IL-6 induction in PMA-differentiated THP-1 human monocytic cells, and (B) IL-6 induction in murine macrophage RAW 264.7 cells. Pam<sub>2</sub>CSK<sub>4</sub> and/or *E. coli* LPS O26 (LPS O26) were used as positive controls. The graphs show the mean  $\pm$  standard error for triplicate values.

### Time-lapse monitoring of internalization of TLR2 ligands in living cells

In order to investigate the intracellular behavior of the fluorescence-labeled TLR2 ligand, Alexa Fluor® 594-labeled Pam<sub>2</sub>CSK<sub>4</sub> (**1a**) and stilbene-Pam<sub>2</sub>CSK<sub>4</sub> (**1e**) were used. We then utilized live-cell imaging combined with a time-lapse monitoring system, and measured with a confocal fluorescence laser scanning microscope equipped with GaAsP multi-detector unit. Ligand concentrations were fixed at 100 nM considering the physiological conditions.

In Fig. 3, the fluorescence (stilbene-type)-labeled Pam<sub>2</sub>CSK<sub>4</sub> (**1e**) was added to HEK293 with or without TLR2/CD14 expression. The ligand internalization and their behavior within cells were recorded every 5 min for 5 h (Fig. 3). When HEK293 cells stably expressing human TLR2/CD14 (HEK-Blue TLR2) were used, the increase of cytosolic labeled-ligands was observed in a time-dependent manner (Fig. 3B), and the results were compared with those from a similar analysis performed on native HEK293 (Fig. 3A). The time-course of ligand accumulation in the cells was measured by following changes in green fluorescence intensity due to **1e**. We observed much higher internalization in the HEK293 expressing TLR2/CD14 compared with wild-type HEK293 (Fig. 3C), over long term monitoring using lower ligand concentrations at 100 nM. In

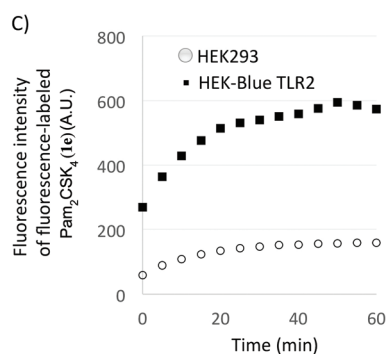
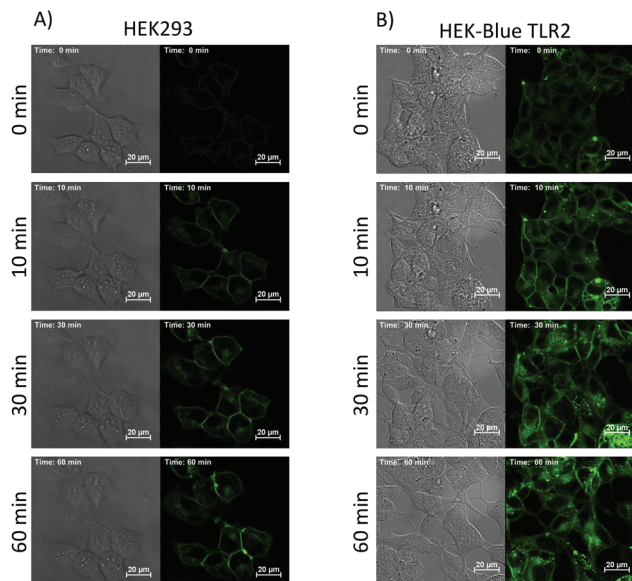


**Fig. 3** Live-cell imaging of fluorescence stilbene-type-labeled Pam<sub>2</sub>CSK<sub>4</sub> (**1e**) endocytosis, either (A) as TLR2/CD14-dependent in HEK-Blue TLR2 or (B) as TLR2/CD14 independent in HEK293. The fluorescence imaging depicts stilbene-Pam<sub>2</sub>CSK<sub>4</sub> (**1e** at 100 nM) in green. (C) Time-course of ligand accumulation in the cells measured by changes in green fluorescence intensity due to stilbene-type-labeled Pam<sub>2</sub>CSK<sub>4</sub> (**1e**). Open circle: HEK293 cells. Filled black square: HEK-Blue TLR2 cells. Fluorescence intensity (A.U.) of Pam<sub>2</sub>CSK<sub>4</sub>-Alexa594 in the whole image was calculated using NIS-Elements AR (Nikon) software.

the case of stilbene-type fluorescence labeling (**1e**), the cell surface was slightly fluorescently visualized even without TLR2 expression as shown in Fig. 3A, and more obviously observed at the cell membrane in HEK-Blue TLR2 as shown in Fig. 3B.

In the case of Pam<sub>2</sub>CSK<sub>4</sub>-Alexa Fluor® 594 (**1a**), the ligand internalization and their behavior within cells were also recorded every 5 min for 5 h, after adding the labeled ligand **1a** with or without the receptor expression (Fig. 4). When HEK293 cells stably expressing human TLR2/CD14 (HEK-Blue TLR2) were used, the increase of cytosolic labeled-ligands was observed in a time-dependent manner (Fig. 4B), and the results were compared with those from a similar analysis performed on native HEK293 (Fig. 4A). The time-course of ligand accumulation in the cells was measured by following changes

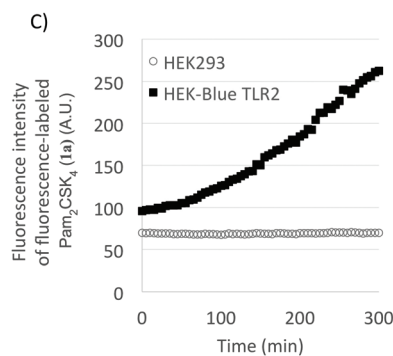
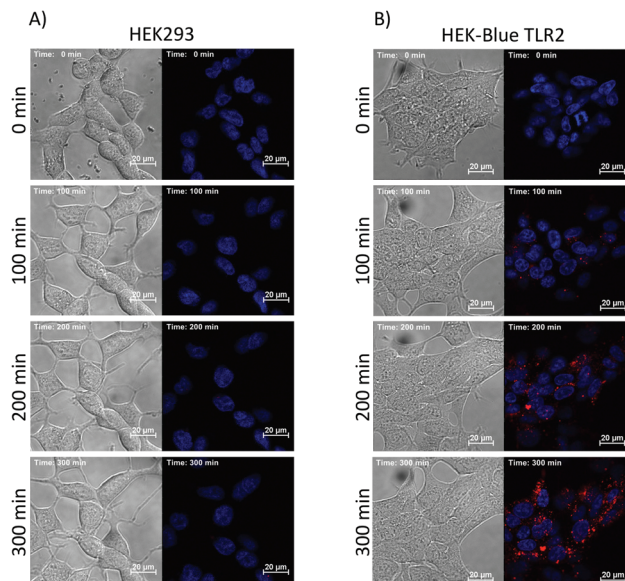


**Fig. 4** Live-cell imaging of fluorescence-labeled Pam<sub>2</sub>CSK<sub>4</sub> (**1a**) endocytosis, either (A) as TLR2 independent in HEK293 or (B) as TLR2/CD14-dependent in HEK-Blue TLR2. Fluorescence imaging depicts Hoechst 33342 staining in blue and Pam<sub>2</sub>CSK<sub>4</sub>-Alexa Fluor® 594 (**1a** at 100 nM) in red. (C) Time-course of ligand accumulation in the cells measured by changes in red fluorescence intensity due to Pam<sub>2</sub>CSK<sub>4</sub>-Alexa594 (**1a**). Open circle: HEK293 cells. Filled black square: HEK-Blue TLR2 cells. Fluorescence intensity (A.U.) of Pam<sub>2</sub>CSK<sub>4</sub>-Alexa594 in the whole image was calculated using NIS-Elements AR (Nikon) software.

in red fluorescence intensity due to **1a**. We observed much higher internalization in the HEK293 expressing TLR2/CD14 compared with wild-type HEK293 (Fig. 4C), over long term monitoring using lower ligand concentrations. In this case, the cell surface was not visualized, in comparison with the hydrophobic stilbene-Pam<sub>2</sub>CSK<sub>4</sub> (**1e**). The different phenomena of the two types of fluorescence-labeled ligands (**1a** and **1e**) are presumably because stilbene-type fluorescence labeling (**1e**) is more easily adsorbed on the cell membrane due to its hydrophobicity, while we also observed higher internalization of both **1a** and **1e** in the HEK293 expressing TLR2/CD14 compared with wild-type HEK293.

The results of their internalization were consistent with previously reported results that showed CD14 dependent internalization of TLR2 ligands.<sup>25</sup> We here succeeded in time-lapse monitoring of the internalization and internal accumulation

of the labeled TLR2 ligands over a long time-course, with utilizing either hydrophilic or hydrophobic fluorescence labeling.

In summary, we were able to observe the behavior of the fluorescence-labeled TLR2 ligand over the course of 5 h as the live-cell imaging over an extended period. In the analysis, we used a highly sensitive detector unit for our confocal imaging microscopy system, which enabled much brighter imaging even with weak fluorescent signals at 100 nM of the labeled ligand.

## Experimental section

### Representative synthesis of fluorescence-labeled TLR2 ligands

The synthetic procedures of other compounds and their spectroscopic data can be found in the ESI.†

**Synthesis of Pam<sub>2</sub>CSK<sub>4</sub> containing the linker.** Pam<sub>2</sub>CSK<sub>4</sub> containing the linker was synthesized by solid-phase peptide synthesis (SPPS) on Rink Amide resin (100–200 Mesh, 81.0 mg, 0.047 mmol) using Fmoc protected amino acids (0.141 mmol) and *N,N'*-diisopropylcarbodiimide (DIC) (21.8  $\mu$ L, 0.141 mmol)/HOBT (19.1 mg, 0.141 mmol) in DMF (800  $\mu$ L). The following protected amino acids were employed: firstly, Fmoc-L-Lys(Dde)-OH (75.1 mg, 0.141 mmol), then, Boc-L-Cys(Trt)-OH (65.4 mg, 0.141 mmol), Fmoc-L-Lys(Boc)-OH (66.1 mg, 0.141 mmol  $\times$  4 times) and Fmoc-L-Ser(Trt)-OH (80.3 mg, 0.141 mmol). Fmoc groups were cleaved by treatment with 20% piperidine in DMF (1 mL, 1 min  $\times$  1, then 20 min  $\times$  1). Dde groups were cleaved by treatment with 5% hydrazine in DMF (1 mL, 1 min  $\times$  1, then 20 min  $\times$  1). The coupling of Fmoc-Pam<sub>2</sub>Cys-OH<sup>3</sup> (84.1 mg, 0.094 mmol) was carried out using DIC (14.6  $\mu$ L, 0.094 mmol) and HOBT (12.7 mg, 0.094 mmol) in DMF (800  $\mu$ L). Progress of the manual couplings was monitored by the standard Kaiser test. After completion of the Pam<sub>2</sub>CSK<sub>4</sub> synthesis, the resin was thoroughly washed with DMF (3 mL), CH<sub>2</sub>Cl<sub>2</sub> (3 mL), and MeOH (3 mL) and dried *in vacuo* to a constant weight. Cleavage of the peptide from the resin was achieved by stirring the resin with a cleavage cocktail composed of trifluoroacetic acid (TFA), CH<sub>2</sub>Cl<sub>2</sub> and triisopropylsilane (TIS) (50 : 50 : 2 = in vol. ratio, 1 mL, 3 min  $\times$  5). The combined solutions were concentrated *in vacuo*. The crude product was purified by HPLC [COSMOSIL 5C<sub>4</sub>-AR-300 Packed column, 220 nm, linear gradient of 75–100% (v/v) of MeOH (0.1% TFA) (solvent B) in H<sub>2</sub>O (0.1% TFA) (solvent A) over 20 min, 1 mL min<sup>-1</sup>] to give the desired compound (23% based on Rink amide resin loading capacity). <sup>1</sup>H NMR (400 MHz, CD<sub>3</sub>OD)  $\delta$  5.27–5.21 (m, 1H), 4.54 (t, *J* = 6.0 Hz, 1H), 4.43 (dd, *J* = 12.0 Hz, 2.4 Hz, 1H), 4.38–4.23 (m, 5H), 4.19–4.09 (m, 3H), 3.92 (dd, *J* = 11.2 Hz, 5.6 Hz, 1H), 3.78 (dd, *J* = 11.2 Hz, 6.4 Hz, 1H), 3.24–3.12 (m, 3H), 3.06–3.04 (m, 2H), 2.94 (t, *J* = 7.2 Hz, 8H), 2.91–2.86 (m, 2H), 2.81 (dd, *J* = 14.4 Hz, 8.0 Hz, 1H), 2.34 (t, *J* = 7.6 Hz, 2H), 2.32 (t, *J* = 7.6 Hz, 2H), 1.95–1.67 (m, 10H), 1.76–1.64 (m, 10H), 1.64–1.56 (m, 4H), 1.56–1.39 (m, 10H), 1.28 (br, 48H), 0.89 (t, *J* = 7.2 Hz, 6H); HRMS (ESI-QTOF MS): calculated for C<sub>74</sub>H<sub>145</sub>N<sub>14</sub>O<sub>13</sub>S<sub>2</sub><sup>+</sup> [M + H]<sup>+</sup>: 1502.0551; found: 1502.0554.

**Synthesis of Alexa-labeled Pam<sub>2</sub>CSK<sub>4</sub> (1a).** To a solution of the liberated Pam<sub>2</sub>CSK<sub>4</sub>-linker (3) (1.0 mg, 0.66  $\mu$ mol) in MeOH (200  $\mu$ L) Alexa Fluor® 594 C5 maleimide (0.40 mg, 0.44  $\mu$ mol) was added. The mixture was stirred under dark conditions overnight, and concentrated *in vacuo*. The resulting mixture was purified by RP-HPLC [COSMOSIL 5C<sub>4</sub>-AR-300 Packed column, 594 nm, linear gradient of 75–100% (v/v) of MeOH (0.1% TFA) (solvent B) in H<sub>2</sub>O (0.1% TFA) (solvent A) over 20 min, 1 mL min<sup>-1</sup>] to give Alexa-labeled Pam<sub>2</sub>CSK<sub>4</sub> (1a) as a solid (0.90 mg, 86%). <sup>1</sup>H NMR (400 MHz, CD<sub>3</sub>OD) 5'-isomer:  $\delta$  8.61 (br, 1H), 8.23 (d, *J* = 8.0 Hz, 1H), 7.40 (d, *J* = 8.4 Hz, 1H), 7.38–7.25 (m, 2H), 6.82 (s, 2H), 5.88–5.86 (m, 2H), 5.26–5.18 (m, 1H), 4.51–4.47 (m, 1H), 4.43–4.38 (m, 1H), 4.37–4.22 (m, 6H), 4.16–4.06 (m, 3H), 3.92–3.82 (m, 1H), 3.79–3.71 (m, 1H), 3.71–3.61 (m, 2H), 3.59–3.54 (m, 2H), 3.52–3.46 (m, 4H), 3.38–3.11 (m, 24H), 2.95–2.84 (m, 10H), 2.79 (dd, *J* = 14.8 Hz, 7.6 Hz, 1H), 2.54 (dd, *J* = 19.2 Hz, 6.4 Hz, 1H), 2.33 (t, *J* = 7.6 Hz, 2H), 2.30 (t, *J* = 7.6 Hz, 2H), 1.95–1.18 (m, 88H), 0.89 (t, *J* = 7.2 Hz, 6H); 6'-isomer:  $\delta$  8.08–7.99 (m, 2H), 7.57 (d, *J* = 8.8 Hz, 1H), 7.38–7.25 (m, 2H), 6.82 (s, 2H), 5.88–5.86 (m, 2H), 5.26–5.18 (m, 1H), 4.51–4.47 (m, 1H), 4.43–4.38 (m, 1H), 4.37–4.22 (m, 6H), 4.16–4.06 (m, 3H), 3.92–3.82 (m, 1H), 3.79–3.71 (m, 1H), 3.71–3.61 (m, 2H), 3.59–3.54 (m, 2H), 3.52–3.46 (m, 4H), 3.38–3.11 (m, 24H), 2.95–2.84 (m, 10H), 2.79 (dd, *J* = 14.8 Hz, 7.6 Hz, 1H), 2.54 (dd, *J* = 19.2 Hz, 6.4 Hz, 1H), 2.33 (t, *J* = 7.6 Hz, 2H), 2.30 (t, *J* = 7.6 Hz, 2H), 1.95–1.18 (m, 88H), 0.89 (t, *J* = 7.2 Hz, 6H); HRMS (ESI-QTOF MS): calculated for C<sub>118</sub>H<sub>192</sub>N<sub>18</sub>O<sub>25</sub>S<sub>4</sub><sup>2+</sup> [M + 2H]<sup>2+</sup>: 1194.6589; found: 1194.6589.

### Inflammatory cytokine induction assay

THP-1 cells were purchased from the Japanese Collection of Research Bioresources (JCRB) Cell Bank (JCRB0112.1). Differentiation of THP-1 cells was induced by incubating 2.0  $\times$  10<sup>5</sup> cells with 0.5  $\mu$ M PMA (InvivoGen) in RPMI-1640 (Nacalai Tesque) supplemented with 10% fetal bovine serum (FBS; Biowest), and 1% penicillin–streptomycin (Gibco) for 24 h.<sup>32</sup> After washing with PBS, the cells were seeded into 96 well plates (3.0  $\times$  10<sup>5</sup> cells per well). After seeding, ligands were added at the indicated concentrations and incubated at 37 °C for 22 h. IL-6 release was measured using an ELISA kit (Affymetrix).

Mouse macrophages (RAW264.7 cells) were purchased from ATCC (TIB-71). These cells were cultured as monolayers in RPMI-1640 (Wako) supplemented with 10% fetal bovine serum (FBS; Gibco), and 1% penicillin–streptomycin (Gibco). The cells were seeded into 96-well plates (5.0  $\times$  10<sup>5</sup> cells per well), and ligands were added at the indicated concentrations before incubation at 37 °C for 24 h. IL-6 release was measured using an ELISA kit (Affymetrix).

### Live cell imaging analysis

The human embryonic kidney 293 (HEK293) and HEK293 stably transfected with human TLR2 and CD14 (HEK-Blue™-hTLR2: obtained from InvivoGen) were incubated in a 35 mm glass-bottom dish with 2 mL Dulbecco's Modified Eagle's medium

(DMEM; Gibco). Ten microliter of either a solution containing a fluorescent organelle marker (either early endosome-GFP, Golgi-GFP, or lysosome-GFP (BacMam 2.0 series obtained from Molecular Probes)) or plain medium was added to the cells before incubation for 16–24 h at 37 °C in 5% CO<sub>2</sub>. Next, 20 μL of solution of Hoechst33342 was then added to the final concentration of 0.1 μM, followed by a 20 min incubation at 37 °C in 5% CO<sub>2</sub>. After washing with either live cell imaging solution (Molecular Probes) or PBS, a solution of 1 μL of fluorescence-labeled TLR2 ligand **1a** in 99 μL of DMEM (0.1 μM final concentration) was introduced, and time-lapse imaging with confocal laser scanning microscopy was performed with a Nikon A1R equipped with a GaAsP detector unit. The setting of imaging conditions is as follows: dimension: 512 × 512 pixel, lens: Plan Apo λ 40× (NA 0.95), scan speed: 1 μs per pixel, laser power: 1.0%, Zoom: 1.00×, excitation wavelength: 405 nm (for Hoechst 33342), 488 nm (for stilbene-Pam<sub>2</sub>CSK<sub>4</sub> **1e**), 561 nm (for Pam<sub>2</sub>CSK<sub>4</sub>-Alexa594 **1a**), excitation dichroic mirror: 405/488/561, emission wavelength: 450 nm (for Hoechst 33342, PMT detector), 525 nm (for **1e**, GaAsP detector), 595 nm (for **1a**, GaAsP detector). Fluorescence intensity (A.U.) of Pam<sub>2</sub>CSK<sub>4</sub>-Alexa594 in the whole image was calculated using NIS-Elements AR (Nikon) software.

## Conclusions

In this study, we developed fluorescence-labeled TLR2 ligands containing either hydrophilic or hydrophobic fluorescence groups. Both types of labeled compounds demonstrated immunomodulatory activities similarly to those of the original unlabeled lipopeptides. We used the representative compounds as the fluorescent probe for live-cell imaging to investigate the dependence of regulation of internalization on TLR2. Live-cell imaging of the TLR2 fluorescence-labeled ligand showed that the TLR2/CD14 expression in the host cells enhanced the internalization of the TLR2 ligand molecules. Our results suggest that expression of TLR2/CD14 modulates the trafficking of its ligands.

## Conflicts of interest

There are no conflicts to declare.

## Acknowledgements

This work was supported by Grants-in-Aid for Scientific Research, KAKENHI (Y. F.; JP26102732, JP26282211, JP17H02207, JP17H05800 and JP16H01162; K. F.; JP26882036, JP23241074, JP15H05836, and JP16H01885) by MEXT-Supported Program (JSPS) for the Strategic Research Foundation at Private Universities (K. K.; S1411010), by NEXT-program from JSPS (Y. F.; LR025), Mizutani Foundation for Glycoscience (Y. F.), Mishima Kaiun Memorial Foundation (Y. F.) and Takeda Science Foundation (Y. F.).

## Notes and references

- 1 E. M. Creagh and L. A. O'Neill, *Trends Immunol.*, 2006, **27**, 352–357.
- 2 M. S. Jin and J. O. Lee, *Immunity*, 2008, **29**, 182–191.
- 3 U. Buwitt-Beckmann, H. Heine, K. H. Wiesmuller, G. Jung, R. Brock, S. Akira and A. J. Ulmer, *J. Biol. Chem.*, 2006, **281**, 9049–9057.
- 4 A. Kovacs-Simon, R. W. Titball and S. L. Michell, *Infect. Immun.*, 2011, **79**, 548–561.
- 5 M. I. Hutchings, T. Palmer, D. J. Harrington and I. C. Sutcliffe, *Trends Microbiol.*, 2009, **17**, 13–21.
- 6 H. Kanzler, F. J. Barrat, E. M. Hessel and R. L. Coffman, *Nat. Med.*, 2007, **13**, 552–559.
- 7 A. G. Jarnicki, H. Conroy, C. Brereton, G. Donnelly, D. Toomey, K. Walsh, C. Sweeney, O. Leavy, J. Fletcher, E. C. Lavelle, P. Dunne and K. H. Mills, *J. Immunol.*, 2008, **180**, 3797–3806.
- 8 N. A. Marshall, K. C. Galvin, A. M. Corcoran, L. Boon, R. Higgs and K. H. Mills, *Cancer Res.*, 2012, **72**, 581–591.
- 9 S. Adams, *Immunotherapy*, 2009, **1**, 949–964.
- 10 K. Hantke and V. Braun, *Eur. J. Biochem.*, 1973, **34**, 284–296.
- 11 K. Tawaratsumida, M. Furuyashiki, M. Katsumoto, Y. Fujimoto, K. Fukase, Y. Suda and M. Hashimoto, *J. Biol. Chem.*, 2009, **284**, 9147–9152.
- 12 K. Kurokawa, H. Lee, K.-B. Roh, M. Asanuma, Y. S. Kim, H. Nakayama, A. Shiratsuchi, Y. Choi, O. Takeuchi, H. J. Kang, N. Dohmae, Y. Nakanishi, S. Akira, K. Sekimizu and B. L. Lee, *J. Biol. Chem.*, 2009, **284**, 8406–8411.
- 13 K. Kurokawa, K. H. Ryu, R. Ichikawa, A. Masuda, M. S. Kim, H. Lee, J. H. Chae, T. Shimizu, T. Saitoh, K. Kuwano, S. Akira, N. Dohmae, H. Nakayama and B. L. Lee, *J. Biol. Chem.*, 2012, **287**, 13170–13181.
- 14 K. Shibata, A. Hasebe, T. Into, M. Yamada and T. Watanabe, *J. Immunol.*, 2000, **165**, 6538–6544.
- 15 A. O. Aliprantis, R. B. Yang, M. R. Mark, S. Suggett, B. Devaux, J. D. Radolf, G. R. Klimpel, P. Godowski and A. Zychlinsky, *Science*, 1999, **285**, 736–739.
- 16 M. Hirschfeld, C. J. Kirschning, R. Schwandner, H. Wesche, J. H. Weis, R. M. Wooten and J. J. Weis, *J. Immunol.*, 1999, **163**, 2382–2386.
- 17 U. Zahringer, B. Lindner, S. Inamura, H. Heine and C. Alexander, *Immunobiology*, 2008, **213**, 205–224.
- 18 Y. Fujimoto, M. Hashimoto, M. Furuyashiki, M. Katsumoto, T. Seya, Y. Suda and K. Fukase, *ChemBioChem*, 2009, **10**, 2311–2315.
- 19 T. Vasselon, P. A. Detmers, D. Charron and A. Haziot, *J. Immunol.*, 2004, **173**, 7401–7405.
- 20 R. Barbalat, L. Lau, R. M. Locksley and G. M. Barton, *Nat. Immunol.*, 2009, **10**, 1200–1207.
- 21 D. M. Underhill, A. Ozinsky, K. D. Smith and A. Aderem, *Proc. Natl. Acad. Sci. U. S. A.*, 1999, **96**, 14459–14463.
- 22 M. Triantafilou, M. Manukyan, A. Mackie, S. Morath, T. Hartung, H. Heine and K. Triantafilou, *J. Biol. Chem.*, 2004, **279**, 40882–40889.

- 23 M. Triantafilou, F. G. Gamper, R. M. Haston, M. A. Mouratis, S. Morath, T. Hartung and K. Triantafilou, *J. Biol. Chem.*, 2006, **281**, 31002–31011.
- 24 N. J. Nilsen, S. Deininger, U. Nonstad, F. Skjeldal, H. Husebye, D. Rodionov, S. von Aulock, T. Hartung, E. Lien, O. Bakke and T. Espevik, *J. Leukocyte Biol.*, 2008, **84**, 280–291.
- 25 K. J. Brandt, C. Fickentscher, E. K. Kruithof and P. de Moerloose, *PLoS One*, 2013, **8**, e80743.
- 26 L. M. Stuart, J. Deng, J. M. Silver, K. Takahashi, A. A. Tseng, E. J. Hennessy, R. A. Ezekowitz and K. J. Moore, *J. Cell Biol.*, 2005, **170**, 477–485.
- 27 M. L. Marre, T. Petnicki-Ocwieja, A. S. DeFrancesco, C. T. Darcy and L. T. Hu, *PLoS One*, 2010, **5**, e12871.
- 28 M. Manukyan, K. Triantafilou, M. Triantafilou, A. Mackie, N. Nilsen, T. Espevik, K. H. Wiesmuller, A. J. Ulmer and H. Heine, *Eur. J. Immunol.*, 2005, **35**, 911–921.
- 29 T. Nakata, M. Yasuda, M. Fujita, H. Kataoka, K. Kiura, H. Sano and K. Shibata, *Cell. Microbiol.*, 2006, **8**, 1899–1909.
- 30 H. M. Shamsul, A. Hasebe, M. Iyori, M. Ohtani, K. Kiura, D. Zhang, Y. Totsuka and K. Shibata, *Immunology*, 2010, **130**, 262–272.
- 31 A. S. Huynh, W. J. Chung, H. I. Cho, V. E. Moberg, E. Celis, D. L. Morse and J. Vagner, *J. Med. Chem.*, 2012, **55**, 9751–9762.
- 32 M. M. Budai, A. Varga, S. Milesz, J. Tozser and S. Benko, *Mol. Immunol.*, 2013, **56**, 471–479.